

Author's pre-print

This work will be submitted to the IEEE for possible publication. Copyright may be transferred without notice, after which this version may no longer be accessible.

Non-uniform Antenna Loading Effect on Embedded Element Patterns and Application to Fault Detection

Georgios Kyriakou

Abstract—A new, iterative algorithm is presented to calculate the Embedded Element Pattern (EEP) transformation from a set of patterns computed for a uniform antenna port loading (scaled identity matrix) to a set of those computed for a non-uniform one (arbitrary diagonal matrix). This method proves particularly useful when inverting the computations to derive the non-uniform entries of the arbitrary load, given the minimum number of EEPs necessary, which dispenses of the redundancy of other matrix-based computations and leads to numerically stable impedance fault calculation. As the EEPs are envisioned to be obtained primarily through measurement, our method is also tested with the inclusion of various noise components and its convergence is evaluated, suggesting the minimum SNR and fading level of the measurement apparatus, as well as the optimal choice of reference antenna to minimise the estimation error.

Index Terms—Embedded Element Pattern, antenna port termination, fault diagnosis, additive-multiplicative noise

I. INTRODUCTION

CHARACTERISATION of antenna arrays for radio astronomy in terms of Embedded Element Patterns (EEPs) under different loading conditions and their subsequent application to beam steering is a well-developed theory [1]. Inverse problems, such as finding the loading condition that leads to specific, usually measured, EEPs are also of interest. This is an important case for fault diagnosis, as the front-end circuitry on which a phased array is mounted can vary because of the failure of low-noise amplifiers (LNAs). This, in turn, is a consequence of environmental effects that are common in operation fields and lead to electrical and mechanical damage or other technical problems. While some solutions have been presented in the literature to identify faulty antennas [2]–[4] using EEPs, a practical algorithm to the problem of calculating faulty termination impedances loading the array has not yet been devised. The EEP transformations from an ideal to an unknown loading condition of an array can be easily inverted to obtain the latter one, but for antenna ports without cross-talk (disjoint antennas) only the N diagonal elements of an impedance load matrix need to be recovered. This practically means there is redundancy in the computation when calculating N non-zero elements using $N \times M$ matrices, where M is the number of simulation or measurement points in the 3D far-field patterns.

To tackle this issue, a perturbative linear algebra derivation has proven useful in computing the new EEPs under faulty termination. Recently, Buck *et. al.* [5] showed that a more complicated relationship arises when each EEP has to be calculated with a different source impedance than that of the passive loading condition of all other elements. To derive such results, a rank-one update of the loaded array admittance matrix was performed. Such a practice is also applicable if one of the passive elements is terminated diversely than all the others, as well as than the source impedance of the EEP at hand. This was comprehensively shown in [6].

In this communication, we revisit this formulation and generalise it employing the loaded array admittance matrix with an aim to

This paper was produced by the IEEE Publication Technology Group. They are in Piscataway, NJ.

Manuscript received Month X, 2026; revised Month XX, 202X.

Georgios Kyriakou is with the University of Rome ‘La Sapienza’, Department of Physics

connect the *nominal* EEPs (loaded with a uniform impedance over all array elements) to the EEPs by loading with an arbitrary non-uniform impedance matrix (all impedances different from each other). This is achieved by a recursive approach of rank-one updates of both the admittance transformation when a new fault becomes present and the new EEP calculation, when the array is loaded with the updated admittance matrix. Wherever possible, circuit or microwave network theory analogues are presented to make sense of the mathematical transformations.

From a practical point of view, Unmanned Aerial Vehicle (UAV) measurements of EEPs have also become an appealing method of aperture array testing, the more such systems become cheaper and more accurate [7]. Aperture arrays for low-frequency radio astronomy, such as the Square Kilometer Array (SKA) and its precursors, could be diagnosed for front-end impedance mismatches using the proposed method, using existing UAV systems [8], [9] and without the need for multiple antennas being measured and using only a reference one. This constitutes an advantage, since reference elements are used for multiple purposes in such arrays. In order for our method to be applicable in this case, robustness with respect to measurement noise has to be demonstrated, similarly as in [10], [11].

The communication is structured as follows: in Sec. II, we review the calculation of [6], its network equivalent and its inversion. We then generalise that calculation for N faults in Sec. III, where we introduce our algorithm. In Sec. IV-A the algorithm is verified using the EEPs of a 16-element tile of the Murchison Widefield Array, while in Sec. IV-B, we introduce additive noise and a fading channel between the measurement probe and the array, and repeat the algorithm calculations for various SNR values (additive noise) as well as channel fading levels (multiplicative noise) to establish its convergence rate and precision to correctly predicting the faulty terminations.

II. EEPs WITH SINGLE FAULTY TERMINATION AND INVERSE IMPEDANCE EQUATION

We begin by stating our notation conventions: boldface is used for vectors and matrices (of each resulting object, after indexing). Indexing is performed as a subscript, “.” denotes all elements of a certain dimension (as is typical in most programming languages). The iteration number of an object is denoted as a superscript. Finally, overbar electric field quantities are vector stacking at sampled far-field points. $\text{diag}(\cdot)$ means the diagonal matrix of the argument, and $(\cdot)^T$ is the matrix-transpose.

We first review the single-fault case of [6] with this updated notation. In an array of N elements, such as that of Fig. 1, element k has a faulty termination load and instead of Z_L it is loaded with an impedance of $Z_F = Z_L + \Delta Z$. We use the Thevenin voltage source equivalent network for EEP calculation characterised by V_g , $Z_g = Z_L$. Considering the n -th element as active and following [5], it is convenient to first calculate the open-circuit currents $I_n^{F,oc} = (\mathbf{Z}_A + \mathbf{Z}_L^k)^{-1} \mathbf{V}_{g,n}$, where $\mathbf{V}_{g,n} = [0 \dots V_g \dots 0]$ with a non-zero entry only at the n -th position, while the load matrix in this case can be written as: $\mathbf{Z}_L^k = Z_L \mathbf{I} + (\Delta Z) \mathbf{u}_k \mathbf{u}_k^T$ where $\mathbf{u}_k = [0 \dots 1 \dots 0]$ a unit vector with an entry at position k . Therefore $I_n^{F,oc} =$

$((\mathbf{Z}_A + \mathbf{Z}_L^k)^{-1} \mathbf{V}_{g,n})_n = V_g \left((\mathbf{Z}_A + Z_L \mathbf{I} + (\Delta Z) \mathbf{u}_k \mathbf{u}_k^T)^{-1} \right)_{:,n}$. For brevity let us define the loaded admittance matrix $\mathbf{Y} = (\mathbf{Z}_A + Z_L \mathbf{I})^{-1}$ of the identically loaded elements, and the loaded admittance matrix $\mathbf{Y}^F = (\mathbf{Z}_A + Z_L \mathbf{I} + (\Delta Z) \mathbf{u}_k \mathbf{u}_k^T)^{-1}$ when antenna k has a faulty termination. By using the Sherman-Woodbury-Morrison formula, the inverse matrix in the column operation can be written as (using also the symmetry property $\mathbf{Y} = \mathbf{Y}^T$):

$$\begin{aligned} \mathbf{Y}^F &= \mathbf{Y} - \frac{(\Delta Z)}{1 + (\Delta Z) Y_{kk}} \mathbf{Y} \mathbf{u}_k \mathbf{u}_k^T \mathbf{Y} \\ &= \mathbf{Y} - \frac{(\Delta Z)}{1 + (\Delta Z) Y_{kk}} \mathbf{Y}_{:,k} \mathbf{Y}_{k,:} \end{aligned} \quad (1)$$

Extracting now the n -th column we have:

$$\begin{aligned} \mathbf{Y}_{:,n}^F &= \mathbf{Y}_{:,n} - \frac{(\Delta Z)}{1 + (\Delta Z) Y_{kk}} (\mathbf{Y}_{:,k} \mathbf{Y}_{k,:})_{:,n} \\ &= \mathbf{Y}_{:,n} - \zeta_k Y_{nk} \mathbf{Y}_{:,k} \end{aligned} \quad (2)$$

where $\zeta_k = (\Delta Z) / (1 + (\Delta Z) Y_{kk})$. The n -th EEP of this formulation is expressed with respect to the oc-EEPs (normalized by the current source I_g) as $E_n^{\mathbf{Z}_L} = V_g / I_g \mathbf{Y}_{n,:}^F \mathbf{E}^{\text{oc}}$ [1]. We then stack all N such row equations in a column, transposing Eq. (2), to get:

$$\begin{aligned} \mathbf{E}^{\mathbf{Z}_L^k} &= \frac{V_g}{I_g} \begin{bmatrix} \mathbf{Y}_{1,:}^F \\ \vdots \\ \mathbf{Y}_{N,:}^F \end{bmatrix} \mathbf{E}^{\text{oc}} \\ &= \frac{V_g}{I_g} \left(\begin{bmatrix} \mathbf{Y}_{1,:} \\ \vdots \\ \mathbf{Y}_{N,:} \end{bmatrix} - \zeta_k \begin{bmatrix} Y_{1k} \mathbf{Y}_{k,:} \\ \vdots \\ Y_{Nk} \mathbf{Y}_{k,:} \end{bmatrix} \right) \mathbf{E}^{\text{oc}} \\ &= \frac{V_g}{I_g} \left(\mathbf{Y}^T - \zeta_k \text{diag}(\mathbf{Y}_{:,k}) \underbrace{[\mathbf{Y}_{:,k} \cdots \mathbf{Y}_{:,k}]^T}_{N \text{ times}} \right) \mathbf{E}^{\text{oc}} \end{aligned} \quad (3)$$

But $V_g / I_g \mathbf{Y}^T \mathbf{E}^{\text{oc}} = \mathbf{E}^{\mathbf{Z}_L}$ [1] and $V_g / I_g [\mathbf{Y}_{:,k} \cdots \mathbf{Y}_{:,k}]^T \mathbf{E}^{\text{oc}} = [E_k^{\mathbf{Z}_L} \cdots E_k^{\mathbf{Z}_L}]^T = E_k^{\mathbf{Z}_L} \mathbf{1}$, where $\mathbf{1} = [1 \dots 1]^T$. Finally:

$$\begin{aligned} \mathbf{E}^{\mathbf{Z}_L^k} &= \mathbf{E}^{\mathbf{Z}_L} - \zeta_k E_k^{\mathbf{Z}_L} \text{diag}(\mathbf{Y}_{:,k}) \cdot \mathbf{1} \\ &= \mathbf{E}^{\mathbf{Z}_L} - \zeta_k E_k^{\mathbf{Z}_L} \mathbf{Y}_{:,k} \end{aligned} \quad (4)$$

The k -th component of these EEPs is the same as calculated in [5], as, indeed, the source impedance is then ‘faulty’ and thus different than that of the passive elements.

Another way to express Eq. (4) is by introducing the open-circuit currents $I_{nk}^{\text{oc}} = Y_{nk} V_g$, which quantify the current induced in port n by excitation of a voltage source V_g on port k with all other ports open-circuited (the ports now refer to the $\mathbf{Z}_A + Z_L \mathbf{I}$ multiport network). If we consider ΔZ as another impedance in series with Z_L in port k (not taken into account in those I^{oc} calculations), then the n -th EEP of Eq. (4) is equal to:

$$E_n^{\mathbf{Z}_L^k} = E_n^{\mathbf{Z}_L} - \frac{Y_{kn} V_g (\Delta Z)}{V_g + Y_{kk} V_g (\Delta Z)} E_k^{\mathbf{Z}_L} \quad (5)$$

$$= E_n^{\mathbf{Z}_L} - \frac{I_{nk}^{\text{oc}} (\Delta Z)}{V_g + I_{kk}^{\text{oc}} (\Delta Z)} E_k^{\mathbf{Z}_L} \quad (6)$$

The factor multiplying $E_k^{\mathbf{Z}_L}$ is the voltage transfer function from an excitation at the now unloaded port n of the $\mathbf{Z}_A + Z_L \mathbf{I}$ multiport network, to what is now seen as the load in port k , namely ΔZ . This concept is also illustrated in Fig. 1, where the red drawings show the contribution of the faulty element expressed by the voltage transfer function. In the special case that $n = k$, the resulting equation is:

$$E_n^{\mathbf{Z}_L^k} = \frac{V_g}{V_g + I_{kk}^{\text{oc}} (\Delta Z)} E_k^{\mathbf{Z}_L} \quad (7)$$

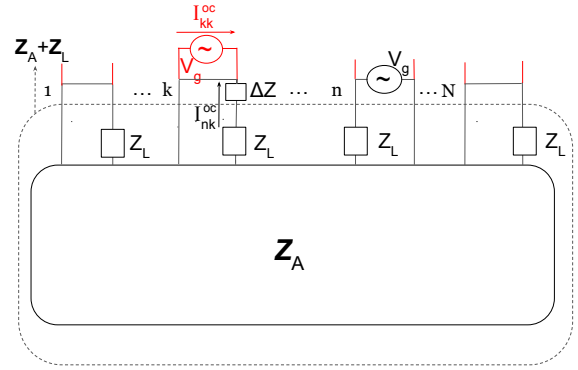


Fig. 1. Network schematic of a Z_L -loaded antenna array of N elements described by its impedance matrix \mathbf{Z}_A , where a faulty element at position k is modelled with an extra series impedance ΔZ along the Z_L termination. The gray lines show the real excitation and termination conditions, while the red lines show the referenced ones for the voltage transfer function of the second term in Eq. (6) (figure adapted from [6]).

In this case the circuit equivalent calculates only the contribution by the open-circuit current on the excited port itself, which in circuit theory is known as a voltage divider.

Using this formula, we can straightforwardly find Z_F from a measurement of the array \mathbf{Z}_L^k -EEPs (under faulty termination), given that the \mathbf{Z}_L -EEPs and the impedance matrix \mathbf{Z}_A are known. Since there is only one unknown, we can take any component $n \in \{1, \dots, N\}$ of Eq. (4) which leads to:

$$E_n^{\mathbf{Z}_L^k} = E_n^{\mathbf{Z}_L} - \frac{(\Delta Z) Y_{nk}}{1 + (\Delta Z) Y_{kk}} E_k^{\mathbf{Z}_L} \Rightarrow \quad (8)$$

$$Z_F = Z_L + \frac{E_n^{\mathbf{Z}_L} - E_n^{\mathbf{Z}_L^k}}{Y_{nk} E_k^{\mathbf{Z}_L} - Y_{kk} (E_n^{\mathbf{Z}_L} - E_n^{\mathbf{Z}_L^k})} \quad (9)$$

As far as the sampling of the electric far-field quantities is concerned, measurement point is needed for this equation to work. Multiple points might nonetheless offer a more robust estimation when measurement uncertainties impact the calculations, by solving a least squares problem as will be shown in the next section.

It is important to also note that the equations presented are agnostic to the form of \mathbf{Y} as the series connection of an antenna impedance matrix with a scaled unity matrix; the perturbation approach also works when applied to a matrix of any other form. We can therefore generalise the single-fault case to achieve impedance fault extraction for any number of faulty loads, by exploiting the same formulation when the matrix \mathbf{Y} is continuously updated from its previous form.

III. EEPs WITH N FAULTY TERMINATIONS AND RECURSIVE INVERSION ALGORITHM

Let us now suppose that there are N faults with respect to the nominal termination, $(\Delta Z)_k$, $k \in \{1, \dots, N\}$, the same as the number of antennas. A similar calculation of the EEPs for this case follows a recursive procedure both for Eq. (1) and Eq. (5). We first introduce the notation:

$$\mathbf{I}^k = \zeta_k \mathbf{Y}_{:,k}^k \quad (10)$$

which is a dimensionless quantity and akin to a reflection coefficient, as will also be seen from the final equation. The superscript ‘F’ is

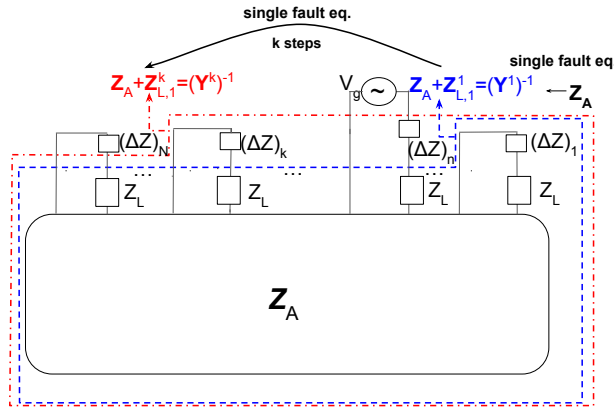


Fig. 2. Schematic representation of the recursion with respect to its progression using impedance matrices. The encircled blocks are defined as impedances, while also expressed as the inverse of the respective admittance matrix presented in the text. Element n radiates, while element k is a sequential element of the recursion.

now dropped from the admittance matrix and replaced by the iteration number. We then follow Eq. (1) recursively, defining:

$$\begin{cases} \mathbf{Y}^0 = \mathbf{Y} \\ \mathbf{Y}^1 = \mathbf{Y}^0 - \Gamma^0 \mathbf{Y}_{1,:}^0 \\ \vdots \\ \mathbf{Y}^N = \mathbf{Y}^{N-1} - \Gamma^{N-1} \mathbf{Y}_{N,:}^{N-1} \end{cases} \quad (11)$$

The general recursive equation is, therefore:

$$\mathbf{Y}^k = \mathbf{Y}^{k-1} - \Gamma^{k-1} \mathbf{Y}_{k,:}^{k-1} \quad (12)$$

We now proceed to calculate recursively the EEPs. First, we introduce the notation: $\mathbf{Z}_{L,1}^k$ to signify a loading matrix where elements 1 through k are faulty. We simplify our previous EEP notation defining: $\mathbf{E}^{\mathbf{Z}_L} = \mathbf{E}^0, \mathbf{E}^{\mathbf{Z}_{L,1}^1} = \mathbf{E}^1, \dots, \mathbf{E}^{\mathbf{Z}_{L,1}^N} = \mathbf{E}^N$. This numbering agrees with the previous admittance matrix numbering, and therefore the Γ numbering as well. Fig. 2 graphically shows how the recursive computation of the new loaded impedance matrices progresses on a schematic of the array loaded with arbitrary loads $Z_L + (\Delta Z)_k, k \in \{1, \dots, N\}$. Equipped with these definitions, we can write down the general, recursive equation based on Eq. (4) as:

$$\mathbf{E}^k = \mathbf{E}^{k-1} - \Gamma^k \mathbf{E}_k^k \quad (13)$$

We subsequently consider successively the n -th component of $\mathbf{E}^n, n \in \{1, \dots, N\}$, and write down Eq. (5):

$$\begin{cases} E_1^1 = E_1^0 - \Gamma_1^1 E_1^0 \\ E_2^2 = E_2^1 - \Gamma_2^2 E_2^1 \\ = E_2^0 - \Gamma_2^1 E_1^0 - \Gamma_2^2 E_2^0 + \Gamma_2^2 \Gamma_1^1 E_1^0 \\ = E_2^0 - \Gamma_2^2 E_2^0 - \Gamma_2^1 (1 - \Gamma_2^2) E_1^0 \\ \vdots \\ E_N^N = E_N^{N-1} - \Gamma_N^N E_N^{N-1} \\ = E_N^0 - \Gamma_N^N E_N^0 - \dots - \Gamma_N^1 \left(\prod_{l=2}^N (1 - \Gamma_l^l) \right) E_1^0 \end{cases}$$

The last, general equation is proven by induction in Appendix A and can be written in a more compact form as:

$$E_N^N = E_N^0 - \sum_{k=1}^N \Gamma_N^k \left(\prod_{l=k+1}^N (1 - \Gamma_l^l) \right) E_k^0 \quad (14)$$

This ‘forward’ equation shows that all Γ_N^k and therefore $\zeta_k, (\Delta Z)_k$ for all $k \in \{1, \dots, N\}$ are used for the calculation of faulty EEP E_N^N . This equation does not provide any advantage with respect to forwardly calculating the EEPs given certain impedance faults, but sets the stage for an algorithm which can perform the inverse calculation, namely calculating the faults given certain sets of EEPs.

We furthermore note that the ordering of the antennas in the above derivation does not matter, and the same expressions apply with different orderings. This is a concept that is best interpreted through signal flow graphs, but proving such an analogy is out of the scope of this paper. However, this observation means the ‘last’, N -th antenna is free to choose, so we will generalise our expressions by replacing N with n , keeping in mind that every time we choose a different reference antenna, some permutation of rows/columns of the respective matrices has to be performed, in order to place it in the N -th position.

To facilitate devising a strategy to calculate $(\Delta Z)_k$, we notice that Eq. (14) is written simply as:

$$E_n^0 - E_n^N = \sum_{k=1}^N T_{k,n} E_k^0 \quad (15)$$

where $T_{k,n} = \Gamma_n^k \left(\prod_{l=k+1}^N (1 - \Gamma_l^l) \right)$. If we know the EEP values at an initial (nominal) and a final (faulty) loading condition at multiple sampled far-field points, the coefficients $T_{k,n}$, which are unknown, can be solved by setting up a system of linear equations when we have at least N such far-field points and solving it using the pseudoinverse matrix (least-squares projection). Then the Γ_n^k coefficients can be retrieved in reverse starting from $\Gamma_n^N = T_{N,n}$ and following backward substitution for $k = N-1, \dots, 1$ as:

$$\Gamma_n^k = \frac{T_{k,n}}{\prod_{l=k+1}^N (1 - \Gamma_l^l)} \quad (16)$$

Finally, we can extract the faults by the definition of ζ_k and taking the n -th component of Eq. (10) as:

$$(\Delta Z)_k = \Gamma_n^k / (Y_{kn}^k - \Gamma_n^k Y_{kk}^k) \quad (17)$$

This is done in incremental numbering, since each $(\Delta Z)_k$ is needed to calculate the new \mathbf{Y}^{k+1} via Eq. (12), including the knowledge of all pre-calculated $\Gamma_n^k, k \in \{1, \dots, N\}$. We only use the n -th Γ^k component in the algorithm, but we then implicitly define all the $n-1$ remaining components to continue the recursion. The algorithm is presented in the form of pseudocode in Alg. 1. The vector (overbar) quantities always refer to a stacking of many (in general $M \geq N$) far-field points along the row dimension, while the column dimension in the matrix quantities has been used to stack the different antenna patterns.

It is worth mentioning that since ultimately every component E_n^N of the final EEPs can be expressed as a linear combination of E_1^0, \dots, E_N^0 , after retrieving the $T_{k,n}$ coefficients, the problem boils down to determining $(\Delta Z)_1, \dots, (\Delta Z)_N$ now as a non-linear function of these entries $T_{k,n}$ and the admittance matrix \mathbf{Y} . This is a computationally hard problem due to the inverse matrix operation involved in the matrix transformation equations of [14]. Symbolic math in numerical codes which can perform such algebra to define the exact non-linear function can easily result in the phenomenon known as ‘expression swell’ for large enough arrays demanding exponentially large calculation costs. Therefore, the recursive approach presented here is well-suited to solving this problem with computational efficiency.

Finally, the algorithm is best implemented when all elements are considered as potentially having a termination fault, and those who

Algorithm 1 Inversion algorithm of Eq. (14) to recover the values $(\Delta Z)_k$, $k \in \{1, \dots, N\}$ using M far-field points

$$\bar{\mathbf{E}}^0 \leftarrow [\bar{E}_1^0 \dots \bar{E}_N^0]$$

$$\mathbf{T} \leftarrow (\bar{\mathbf{E}}^{0,\text{T}} \bar{\mathbf{E}}^0)^{-1} \bar{\mathbf{E}}^{0,\text{T}} \cdot (\bar{E}_n^0 - \bar{E}_n^N)$$

$$\Gamma_n^N \leftarrow T_{N,n}$$

for $k = N - 1, 1, 1$

$$\Gamma_n^k = \frac{T_{k,n}}{\prod_{l=k+1}^N (1 - \Gamma_n^l)}$$

end

$$\mathbf{Y}^1 = (\mathbf{Z}_A + Z_L \mathbf{I})^{-1}$$

for $k = 1, 1, N - 1$

$$(\Delta Z)_k \leftarrow \Gamma_n^k / (Y_{kn}^k - \Gamma_n^k Y_{kk}^k)$$

$$\mathbf{Y}^k \leftarrow \frac{(\Delta Z)_k}{1 + (\Delta Z)_k Y_{kk}^k} \mathbf{Y}^k$$

$$\mathbf{Y}^{k+1} \leftarrow \mathbf{Y}^k - \mathbf{\Gamma}^k \mathbf{Y}_{k,:}^k$$

end

$$(\Delta Z)_N \leftarrow \Gamma_n^N / (Y_{Nn}^N - \Gamma_n^1 Y_{NN}^1)$$

do not present such deviation from the nominal value will result in $\Delta Z = 0$ up to a certain tolerance.

IV. NUMERICAL VALIDATION

A. Simulated patterns without noise

We will first test our algorithm with a simulated array to establish possible numerical errors, which are known to accumulate in recursive computations. We also remind the reader that any single EEP of those under faulty termination can be used as the right hand side of Eq. (15), so this parameter will also be assumed free, in order to examine the effect of such a ‘reference’ EEP and whether the particular geometric placement of its corresponding array element has any effect. Let us denote this ‘reference’ antenna number n , while the number of the antenna for which the new termination is estimated will be denoted k . The true terminations used are denoted $Z_{F,k}^{\text{true}}$, while the estimated ones will be $Z_{F,k}^{\text{alg},n}$.

As in [6], we will use as an example a 16-element tile of the Murchison Widefield Array (MWA) [12]. This radio astronomical array is situated at Inyarrimanka Ilgari Bundaya, a radio quiet zone in Western Australia, and conducts low-frequency science in the 70 to 300 MHz band. The electromagnetic characterisation for such a tile, which is a 4×4 subarray within the instrument, has extensively been treated in [13]. We will consider the MWA tile EEPs at 128 MHz with a nominal termination of $Z_L = 50 \Omega$, while faults will be introduced at 4 positions of the array, such that: $Z_{F,1}^{\text{true}} = 28.87 + j15.98 \Omega$, $Z_{F,6}^{\text{true}} = 19.9 + j11.01 \Omega$, $Z_{F,11}^{\text{true}} = 21.6 + j11.96 \Omega$ and $Z_{F,16}^{\text{true}} = 13 + j7.2 \Omega$. These correspond to real measurements of faulty LNA input impedances mounted on the MWA tile elements [14].

Fig. 3 shows the absolute error between true and algorithmically estimated values of the faulty termination impedance of antenna k using the reference EEP of antenna n and a sampling of the 3D far-field described by the sets $\Omega_\theta = \{n_\theta \cdot 5^\circ, n_\theta = 0, \dots, 9\}$ and $\Omega_\phi = \{n_\phi \cdot 45^\circ, n_\phi = 0, \dots, 7\}$. As can be seen from this plot, higher errors are observed when using the 5-th, 7-th or 12-th antenna as reference, while all other choices generally lead to errors of less than 4Ω . The best reference antenna is the 4-th one, with an RMS error over all faults equal to 0.21Ω (or 1.91% normalized). It is

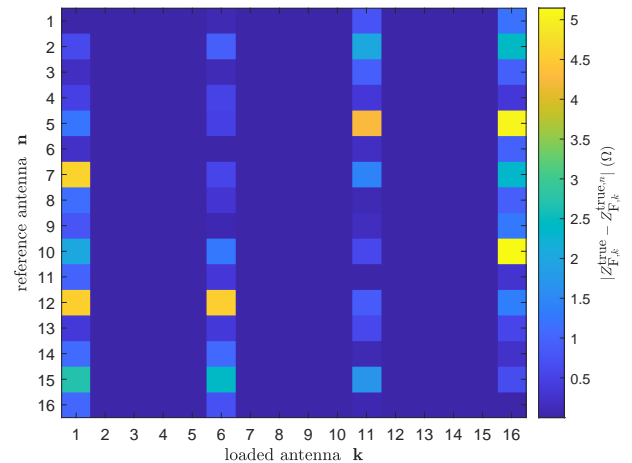


Fig. 3. Discrete color grid of the absolute error value using the far-field sampling $\Omega_\theta \times \Omega_\phi$, of the estimations of the faulty termination impedance of antenna n using the reference EEP of antenna k .

also observed that the algorithm always predicts where a fault does not exist: if we exclude columns 1, 6, 11, 16 from Fig. 3 (where the loaded antennas do have a fault), then the maximum error is $1.5 \times 10^{-7} \Omega$.

As far as the computation time is concerned, as can be seen from Alg 1, the complexity is $\mathcal{O}(N^3)$, defined both by the \mathbf{Y}^1 computation as well as the N iterations of the $\mathbf{\Gamma}^k \mathbf{Y}_{k,:}^k$ computation (we consider the standard and not accelerated matrix operation complexities). Using Matlab on a Lenovo laptop with an Intel Core 7, 10-core processor at 1.8 GHz and 32 GB of RAM, the time elapsed for one full computation is 0.0062 seconds. Attempts at solving the problem using optimisation methods on the non-linear expression of $T_{k,n}$ ’s derived through symbolic math and substituted to Eq. (15) did not give convergent results, while at the same time requiring a computation time between 15-30 seconds.

B. Simulated patterns with additive and multiplicative noise

Since the method presented is of potential use with measurement data, the case of non-ideal EEPs will be examined. The scattering matrix will in this section also be considered fully known; this ideal condition should in fact also be further examined according to errors that can occur in indirect determination of this matrix, as has been studied in [11]. In order to model a potential measurement of an EEP, we introduce a complex Gaussian additive noise term, which is drawn from the Gaussian distribution parametrised by the Signal-to-Noise Ratio (SNR). We furthermore implement 1000 realizations of that term per each SNR point examined and average the resulting squared errors computed, so as to ensure statistically unbiased results. Thus, the noise term is described as:

$$w_k \sim \mathcal{N}_r(0, \sigma_k) + j\mathcal{N}_i(0, \sigma_k), \quad \sigma_k = \sqrt{\frac{\eta_0 P_k}{\text{SNR}}} \quad (18)$$

where P_k is the radiated power corresponding to the k -th EEP and the r, i indices of the normal distribution random variables signify different realisations of the real and imaginary part (seeds in statistical terminology) and η_0 is the free-space impedance.

In this case, the number of antenna pattern chosen from the array at faulty conditions, n , will be examined both by averaging over all possible elements and by choosing the one that minimises the current error, that is, the RMS of errors of the estimated termination

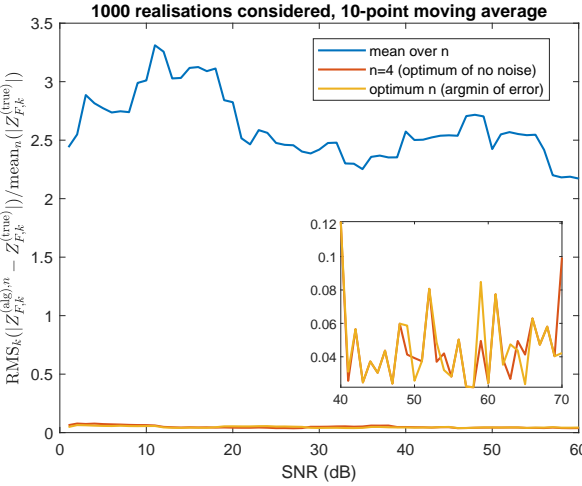


Fig. 4. RMS error versus SNR of true with respect to algorithmically estimated termination impedance, normalised over the mean of all impedances and smoothed with a 10-point moving average across the SNR range, for a 16-element MWA tile over 1000 realisations of additive Gaussian noise. Results are either shown averaged over computations for each reference element n , for the case of $n = 4$ or for the optimum EEP n that most frequently minimises the RMS across all 1000 realisations. A brief inset (with no moving average) also shows the high-SNR trend of the last two cases.

impedances at a certain SNR. This antenna will be selected as the one which most frequently minimises such an error across all 1000 realisations of the computation. In these realisations, we also randomly re-arrange all other elements in positions 1 through $N - 1$ (while placing the n -th at position N), in order to get an impartial result independent of the MWA array element numbering.

Fig. 4 presents the RMS of the estimations of the faulty termination impedance over all antennas as a function of the SNR (in dB), either by taking the RMS again over the computations performed with each reference antenna $n \in \{1, \dots, N\}$ ('mean over n ') or by just using the n that most frequently minimises the error across all 1000 realisations ('optimum n '). The case of $n = 4$ is also plotted for comparison, as it has been found to be the optimum n in the noiseless EEP case. The result is normalised over the mean value of the $|Z_{F,k}^{\text{true}}|$, $k \in \{1, \dots, N\}$ while a moving 10-point average has been applied across the SNR values to smooth out large values produced by divergent implementations, that bias certain SNR points (even with such a large number of implementations).

It can be seen that, when computing the normalised RMSE in an average sense over all possible reference elements, the error attains a very high value that never converges, but fluctuates around 250%. When a fixed element that minimises the error is chosen to perform the computation, the error is mostly flat to a low normalised RMSE (4%), even for $\text{SNR} > 10$ dB. This element is one of the following, depending on the SNR: 1st, 4th or 13th, as has been verified by keeping the 'argmin' indices during the simulation. The $n = 4$ case presents roughly the same behaviour, meaning that this element can be chosen as the constant reference independently of the SNR. According to the original numbering of an MWA tile, these are 3 of the 4 elements at the vertices of the rectangular array configuration; the 16-th one, which is at the fourth vertex, has also been verified to lead to a similarly low RMSE. We further report that with the original ordering of the MWA antennas, lower errors could be observed; we choose to report here the generalised case where the antenna arrangement is decided randomly and does not reflect the geometric position of each element within the array.

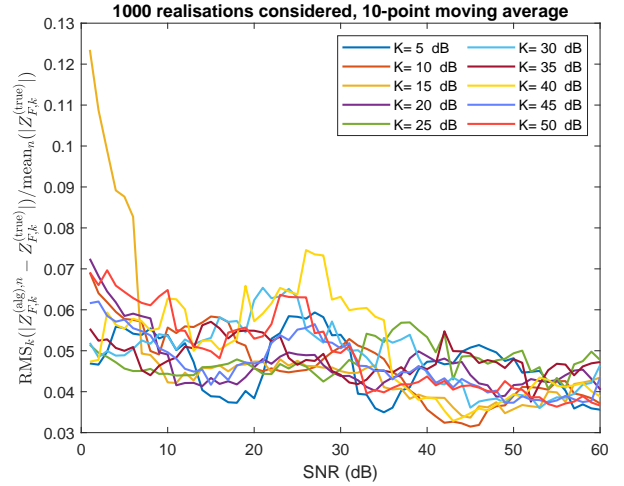


Fig. 5. RMS error versus SNR of true with respect to algorithmically estimated termination impedance, normalised over the mean of all impedances and smoothed with a 10-point moving average across the SNR range, for a 16-element MWA tile over 1000 realisations of additive Gaussian noise and multiplicative Rician fading. The fading level K of each curve is reported in the legend. Only the 'optimum n ' curves are shown here.

As a more complete model, the next step is to introduce multiplicative noise, which models the fading nature of the line-of-sight channel when a transmitter probe and the antenna-under-test as receiver interact in a measurement scenario. Such behavior is modelled by a Rician distribution of the multiplicative factor $g_k \sim \mathcal{R}(\nu_k, \sigma_{R,k})$ that affects the amplitude of the received embedded element pattern E_k^m , $m \in \{0, n\}$ ('0' nominal and 'n' for faulty). The phase is assumed to be known and better controlled, as various techniques ensure its correct retrieval with respect to the reference antenna [15]. As has also been practiced in [11], we can use a normalised channel amplitude factor so as to have $\mu_{R,k} = 1$, from which we can derive ν_k , $\sigma_{R,k}$ using the Rician distribution formula for the mean value of g_k . The fading level of the channel is usually expressed by the factor $K = \nu_k^2 / (2\sigma_{R,k}^2)$. Our model now reads:

$$\hat{E}_k^m = g_k E_k^m + w_k \quad (19)$$

where \hat{E}_k^m refers to the measured EEP. Subsequently, we implement this model using 1000 noise realisations for each pair of (SNR, K) while sampling K at sparser values (from 5 to 50 with a step of 5). Fig. 5 shows the normalised RMS error vs SNR (in dB) for all tested K (in dB), as in Fig. 4, only for the 'optimum n ' case (in these simulations, too, the 'optimum n ' coincides with one of the lateral tile elements). It can be seen that, as with the case of no fading ($K \rightarrow \infty$), for high SNR ($\text{SNR} > 40$ dB) the error converges to a low value less than 5%, but deviations to around 8% are still observed especially for fading levels $K < 30$ dB. As has also been seen in [11], there is no clear trend of the RMSE by increasing the K value. It is therefore more important to keep a high SNR value than to ensure a non-fading channel, in order to obtain accurate results.

V. CONCLUSIONS

An algorithm that computes impedance faults of the front-end termination of N -element array antennas has been described, using a full set of EEPs at the nominal termination impedance, and one EEP at non-uniform (faulty) termination. Using simulated EEPs from a 16-element tile of a radio-astronomical array, the algorithm correctly finds the impedance fault at an accuracy of around 2%; that error is higher when noise is added in our model to estimate how a measured

EEP would affect the calculation and the algorithm then converges to around 4% for high signal-to-noise ratio and fading channel levels. In our example, the vertex elements of the rectangularly arranged array are the ones that achieve the minimum error when their EEP is chosen as the right-hand-side of the least-squares problem with which the algorithm starts; more configurations would need to be tested to ascertain whether such lateral elements are always the optimum choice for our proposed method. Our results show that the algorithm can reliably be applied in radio astronomical antenna arrays for fault detection of individual elements' front-end impedance using the minimum number of EEP measurements.

APPENDIX PROOF OF EQ. (14)

We prove here the general form of Eq. (14) for a N -element array using induction, where m is the integer number of the recursion step. For $m = 1$, the product is by definition equal to 1 (since the upper limit is lesser than the lower limit) and the equation reduces to:

$$\begin{aligned} E_n^1 &= E_n^0 - \sum_{k=1}^1 \Gamma_n^k \left(\prod_{l=k+1}^1 (1 - \Gamma_n^l) \right) E_k^0 \\ &= E_n^0 - \Gamma_n^1 E_1^0 \end{aligned} \quad (20)$$

This is the equation of the single case, proven in Sec. II. We now suppose that Eq. (14) holds when the integer step $1 \leq m \leq N-1$ is considered for all $n \in \{1, \dots, N\}$, and examine its form for $m+1$:

$$\begin{aligned} E_n^{m+1} &= E_n^0 - \sum_{k=1}^{m+1} \Gamma_n^k \left(\prod_{l=k+1}^{m+1} (1 - \Gamma_n^l) \right) E_k^0 \\ &= E_n^0 - \Gamma_n^{m+1} E_{m+1}^0 - \sum_{k=1}^m \Gamma_n^k \left(\prod_{l=k+1}^{m+1} (1 - \Gamma_n^l) \right) E_k^0 \end{aligned}$$

Since for $k \leq m \Rightarrow k+1 \leq m+1$, all terms of the sum have the factor $1 - \Gamma_n^{m+1}$ as their common one, so the above equation takes the form:

$$\begin{aligned} E_n^{m+1} &= E_n^0 - \Gamma_n^{m+1} E_{m+1}^0 - \sum_{k=1}^m \Gamma_n^k \left(\prod_{l=k+1}^m (1 - \Gamma_n^l) \right) E_k^0 \\ &\quad + \Gamma_n^{m+1} \sum_{k=1}^m \Gamma_n^k \left(\prod_{l=k+1}^m (1 - \Gamma_n^l) \right) E_k^0 \end{aligned} \quad (21)$$

By virtue of the assumption that the equation hold for integer m , the first plus third terms can be substituted by E_n^m so that:

$$E_n^{m+1} = E_n^m - \Gamma_n^{m+1} \left(E_{m+1}^0 - \sum_{k=1}^m \Gamma_n^k \left(\prod_{l=k+1}^m (1 - \Gamma_n^l) \right) E_k^0 \right) \quad (22)$$

We now set $n = m+1$ and note that the term in parenthesis is again by the same assumption equal to E_{m+1}^m , such that we obtain:

$$E_{m+1}^{m+1} = E_{m+1}^m - \Gamma_{m+1}^{m+1} E_{m+1}^m \quad (23)$$

But this equation is the general, rank-one update on the $(m+1)$ -th EEP, which has been proven in Sec. II. Eq. (14) in the main text is the application of this equation when $m+1 = N$ but it has been claimed to be valid for all n . As has also been emphasized in the text, we can now re-arrange the ordering of the antennas and ensure that the last, N -th element is one that has not been placed last in any previous ordering. Since the induction assumption is valid for any $n \in \{1, \dots, N\}$, the above procedure can be repeated without further assumptions, where now the Γ_{m+1}^k , $k \in \{1, \dots, N\}$ are different factors. Hence the proof is complete.

ACKNOWLEDGMENTS

I would like to thank Karl F. Warnick and Tobia Carozzi for having read earlier versions of the manuscript and provided useful comments. I also thank Maria Kovaleva for having provided the MWA tile simulated EEPs. I acknowledge the Wajarri-Yamatji people as the traditional owners of the observatory site where Murchison Widefield Array operates; and all indigenous peoples' right to their land.

REFERENCES

- [1] K. F. Warnick, D. B. Davidson and D. Buck, "Embedded Element Pattern Loading Condition Transformations for Phased Array Modeling," in *IEEE Transactions on Antennas and Propagation*, vol. 69, no. 3, pp. 1769-1774, March 2021, doi: 10.1109/TAP.2020.3027593.
- [2] K. P. Prajosh, S. S. Ranganathan, F. Ferranti, and U. K. Khankhoje, "Efficient mutual-coupling aware fault diagnosis of phased array antennas using optimized excitations", in *IEEE Antennas and Wireless Propagation Letters*, vol. 21, no. 9, pp. 1906-1910, 2022
- [3] J. A. Rodriguez-Gonzalez, F. Ares-Pena, M. Fernandez-Delgado, R. Iglesias, and S. Barro, "Rapid method for finding faulty elements in antenna arrays using far field pattern samples," in *IEEE Transactions on Antennas and Propagation*, vol. 57, no. 6, pp. 1679-1683, 2009
- [4] H. M. Yao, M. Li, L. Jiang, K. L. Yeung and M. Ng, "Antenna array diagnosis using a deep learning approach", in *IEEE Transactions on Antennas and Propagation*, vol. 72, no. 6, pp. 5396-5401, 2024
- [5] D. Buck, K. F. Warnick, R. Maaskant, D. B. Davidson and D. F. Kelley, "Measuring Array Mutual Impedances Using Embedded Element Patterns," in *IEEE Transactions on Antennas and Propagation*, vol. 71, no. 1, pp. 606-611, 2023
- [6] G. Kyriakou, M. Kovaleva and D. B. Davidson, "Impact of Antenna Load on Embedded Element Patterns in Aperture Arrays: the Single Fault Case," in *2024 4th URSI Atlantic Radio Science Meeting (AT-RASC)*, Meloneras, Spain, 2024, pp. 1-4, doi: 10.46620/URSIATRASC24/KLRW4510
- [7] V. R. Kandregula, Z. D. Zaharis, Q. Z. Ahmed, F. A. Khan, T. H. Loh, J. Schreiber, A. J. R. Serres and P. I. Lazaridis, "A Review of Unmanned Aerial Vehicle Based Antenna and Propagation Measurements", in *Sensors*, 2024, 24, 7395, <https://doi.org/10.3390/s24227395>
- [8] L. Ciorba *et al.*, "Electromagnetics-Aware Path for UAV-Based Near-Field Antenna Measurements Implemented With a High Dynamic Range SDR," in *IEEE Transactions on Instrumentation and Measurement*, vol. 73, pp. 1-13, 2024, Art no. 8005513, doi: 10.1109/TIM.2024.3476517
- [9] Z. Weng, C. Liang, G. Sun, F. De Paulis, R. Waterhouse, Y. Qi, and Y. C. Jiao, "A Sparse Near-Field Measurement Technology for SKA-Low Antenna System," in *IEEE Transactions on Instrumentation and Measurement*, vol. 74, pp. 1-14, Art no. 8003914, doi: 10.1109/TIM.2025.3555738
- [10] M. Kovaleva and K. F. Warnick, "Effect of Noise in Embedded Element Pattern Measurements on Mutual Impedance Matrix Extraction," in *2023 17th European Conference on Antennas and Propagation (EuCAP)*, Florence, Italy, 2023, pp. 1-3, doi: 10.23919/EuCAP57121.2023.10133058
- [11] G. Kyriakou, M. Kovaleva, K. F. Warnick, D. B. Davidson and P. Bolli, "Deriving Mutual Impedance Matrix of a Large Antenna Array From Embedded Element Patterns With Measurement Noise," in *IEEE Transactions on Antennas and Propagation*, vol. 73, no. 1, pp. 216-224, Jan. 2025, doi: 10.1109/TAP.2024.3470311
- [12] R. B. Wayth, S. J. Tingay, C. M. Trott *et al.*, "The Phase II Murchison Widefield Array: Design overview," in *Publications of the Astronomical Society of Australia*, 2018; 35:e033, doi:10.1017/pasa.2018.37
- [13] A. Sutinjo, J. O'Sullivan, E. Lenc, R. B. Wayth, S. Padhi, P. Hall and S. T. Tingay, "Understanding instrumental Stokes leakage in Murchison Widefield Array polarimetry", in *Radio Science*, vol. 50, no. 1, pp. 52-65, 2015, doi: 10.1002/2014RS005517
- [14] M. Kovaleva, D. Ung, A. Sutinjo, B. Juswardy, D. B. Davidson and R. B. Wayth, "Analysis of the Loading Effect of Faulty LNAs on Embedded Element Patterns in the Murchison Widefield Array," in *14th European Conference on Antennas and Propagation (EuCAP)*, Copenhagen, Denmark, 2020, pp. 1-4, doi: 10.23919/EuCAP48036.2020.9135727
- [15] L. Ciorba *et al.*, "Understanding phase pattern discrepancies in UAV-based measurements of a SKA-low prototype," in *2022 16th European Conference on Antennas and Propagation (EuCAP)*, Madrid, Spain, 2022, pp. 1-4, doi: 10.23919/EuCAP53622.2022.9769386